Chapter 16
Sliding Mode Control in Heavy Vehicle Safety

H. Imine and L. Fridman

Abstract. In this chapter, an original approach to heavy vehicles rollover risk prediction is presented and validated experimentally. It is based on the calculation of the LTR (Load Transfer Ratio) which depends on the estimated vertical forces using high order sliding mode observers. Previously, a tractor model is developed. The validation tests were carried out on an instrumented truck rolling on the road at various speeds and lane-change manoeuvres. Many scenarios have been experienced: driving straight, curved trajectories, zigzag manoeuvre and brake tests to emphasize the rollover phenomenon and its prediction to set off an alarm for the driver. In this study, the vehicle dynamic parameters (masses, inertias, stiffness..) and the static forces infrastructure characteristics (road profile, radius of curvature, longitudinal and lateral slope, skid resistance) are measured or calculated before the tests.

Key words: Heavy vehicle modeling, Rollover, Sliding mode observer, Estimation, Prediction.

16.1 Introduction

Statistics show that accidents related to heavy goods vehicle (HGV) are more dangerous than those of passenger vehicles ([[39]], [[13]]). While they constitute only

H. Imine
LEPSIS-IFSTTAR, Laboratory for road operation, perception,simulators and simulations, The French institute of science and technology for transport, development and networks, Paris, 75732, France
e-mail: hocine.imine@ifsttar.fr

L. Fridman
UNAM, Departamento de Ingeniería, de Control y Robótica División de Ingeniería Eléctrica, Facultad de Ingeniería UNAM, Mexico
e-mail: lfridman@servidor.unam.mx

B. Bandyopadhyay et al. (Eds.): *Advances in Sliding Mode Control*, LNCIS 440, pp. 313–340.
DOI: 10.1007/978-3-642-36986-5_16

3% of vehicles in traffic, heavy vehicles are involved in 10% of accidents with fatalities. Furthermore, the fatality rate is twice as high when a HGV is involved. Rollover is one of the most frequent accidents (20%) and causes significant damage to the vehicles and injuries to its driver and passengers. Several anti-rollover systems and rollover warning systems were developed to assist or warn the driver ([4], [1], [18]). Most of the current prevention systems have some limitations, because they are based on real time measurements without any prediction of the vehicle dynamics. When the HGV behavior and infrastructure are well known, it is possible to be closer to the safety limit while maintaining an acceptable risk level. But with less information, the rollover risk increases, and the driver must reduce its risk by reducing the vehicle speed. Therefore, it is important to take into account the most relevant uncertainties and parameters variations of heavy vehicle system.

As mentioned in ([7], [25]), the rollover occurs when the lateral acceleration equals or exceeds the vehicle's rollover limit (which may be assisted by roadway cross-fall or camber). Lateral acceleration in a curve is highly sensitive to speed. The required speed to produce rollover reduces as the radius of curvature reduces. Roll stability is influenced by the centre of gravity height (COG), the effective track width provided by the axles and tires, and the suspensions characteristics. The COG height is affected by the chassis height and the heavy vehicle load. This performance measure is evaluated in terms of the steady-state lateral acceleration at which all wheels on the inside of curvature have lifted off the road surface. This is accomplished by increasing the steer angle of a vehicle until all axles on one side of a given vehicle lift off. The rollover can occur when one wheel of the same axle of the vehicle, lifts off the road surface. Previous work was done on rollover of heavy vehicles and several simulation results were presented ([19], [5], [31], [23], [41], [25]). Most of these works have not presented experimental results. Indeed, the instrumentation of a heavy vehicle is very expensive and not easily reached to all. In this chapter, the first experimental results of a developed predictive rollover system of heavy vehicle are presented.

The predictive system is based on the calculation of the Load Transfer Ratio (LTR) which is an indicator of rollover stability. This LTR is defined as the proportion of load on one side of a vehicle unit transferred to the other side in a transient manoeuvre. Thus, it depends on vertical forces that are estimated via a third order sliding mode observer ([24], [22], [25]). It estimates in the same and finite time, positions, speeds and accelerations of the heavy vehicle ([36], [37], [16], [17], [9], [28]). Many researches have been performed in order to estimate vertical forces of the vehicle and many simulation results are presented ([26], [33]). However, in these works, the dynamic parameters of the vehicle are supposed well known which is not always true. Khemoudj et al [32] have developed method to estimate vertical forces without knowledge of dynamic parameters. However, in these works the validation is done only with simulations using software simulator. In this work some of dynamic parameters, namely suspension stiffness and unsprung mass have been identified. This identification permits to improve the quality of the estimation ([40], [14]). One notices also that most of the published works presented only simulation results without real validation using an instrumented vehicle. This

is due to the fact that the instrumentation of vehicle using the existing devices is expensive and difficult to install (more information in the site *www.kistler.com*).

In the presence of uncertainties and perturbation, the sliding mode observer is proved to be the most interesting tool ([[2]], [[43]]). The observer outputs are the estimated state variables of the vehicle (positions and especially the COG height, speeds and accelerations). Then the vertical forces acting on the wheels, which depend on the road inputs are deduced from these estimated variables. In order to show the effectiveness of the proposed system, some validation tests were carried out on an instrumented truck driving on the road at various speeds and maneuvers. Many scenarios have been experienced: driving in straight line, in curve, zigzag and brake tests to emphasize the rollover phenomenon and its prediction and send an alarm to the driver with recommended speed in order to avoid the rollover. This chapter is organized as follows: the second section is devoted to the description of the heavy vehicle model. In the third section, identification of uncertainties and perturbations of heavy vehicle is developed. In section four, the used sliding mode observer to predict rollover is developed. Instrumented heavy vehicle is described in the section four. In section five, some validation results are presented. Finally some conclusions and perspectives are given in the last section.

16.2 System Modelling

Various studies have dealt with the heavy vehicle modeling taking into account the infrastructure characteristics ([[3]], [[6]], [[1]], [[20]], [[26]]). To go in this way, the measurements carried out on the real vehicle are exploited in order to constitute a database which was used to study the various driving risks such as rollover or jack-knifing. In this part, a heavy vehicle model using the infrastructure database is developed. A tractor with 2 axles and 5 degrees of freedom is considered and represented in figure 16.1.

The tractor chassis (with the mass M) is suspended on its axles through two suspension systems. The tire of the wheel i is modeled by the springs with coefficients k_i and the suspension is modeled by both springs with coefficient K_i and damper elements B_i.

The suspension is modeled as the combination of spring and damper elements. The front view of this model is shown in figure 16.2.

The wheel masses are given by m_i $(i = 1, \cdots, 4)$. At the tire contact, the road profile, longitudinal and lateral slope, skid resistance and radius of curvature are considered as the inputs of the system. The road profile is represented by the variable u_i $(i = 1, \cdots, 4)$. The relative yaw and pitch angles of the heavy vehicle are neglected. Therefore, the dynamic model of the vehicle derived from the Lagrangian's equations is given by:

$$M(q)\ddot{q} + B(q,\dot{q})\dot{q} + K(q) = F_g \tag{16.1}$$

Fig. 16.1 Instrumented heavy vehicle

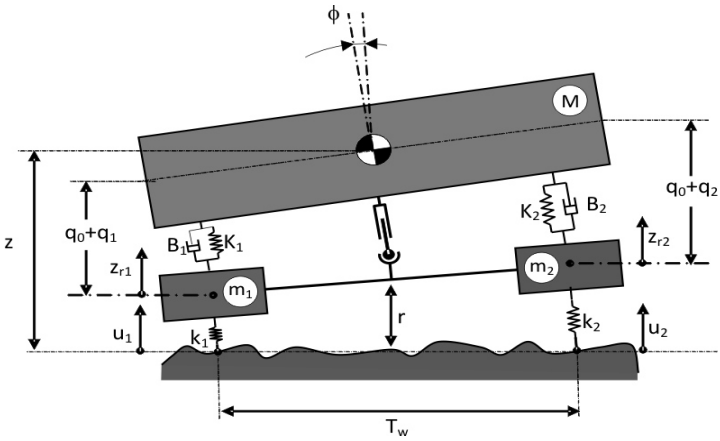

Fig. 16.2 Suspension model

where $M \in \Re^{5\times5}$ is the inertia matrix (mass matrix), $B \in \Re^{5\times5}$ is the matrix taking into account the damping effects, $K \in \Re^5$ is the springs stiffness vector and $F_g \in \Re^5$ is the generalized forces. The coordinates variable vector $q \in \Re^5$ is defined by:

$$q = [q_1, q_2, q_3, q_4, \phi]^T \tag{16.2}$$

where q_1 and q_2 are respectively the left and right front suspension deflection of the tractor, q_3 and q_4 are respectively the left and right rear suspension deflection of

the tractor and ϕ is the roll angle. The vertical acceleration of the chassis (tractor's body) is function of vector q and its time derivative $\dot{q}$:

$$\ddot{z} = f(q, \dot{q}) \tag{16.3}$$

where the variable z is the vertical displacement of the tractor sprung mass which is the centre height of the gravity. The vertical displacements of the wheels with respect to the ground (road) are represented by z_{ri} $(i = 1, \cdots, 4)$ and can be calculated as follows:

$$\begin{cases} z_{r1} = z - (q_0 + q_1) + \frac{T_w}{2}\sin(\phi) - r \\ z_{r2} = z - (q_0 + q_2) - \frac{T_w}{2}\sin(\phi) - r \end{cases} \tag{16.4}$$

where q_0 is the static distance between the COG and the axles of the vehicle, T_w is the tractor track width and r is the wheel's radius. From equation (16.4), the centre height of gravity z is as follows :

$$z = \frac{1}{2}(z_{r1} + z_{r2} + q_1 + q_2) + q_0 + r \tag{16.5}$$

The vertical accelerations of the wheels are obtained using the following equations:

$$\begin{cases} \ddot{z}_{r1} = (B_1\dot{q}_1 + K_1\frac{T_w}{2}\sin(\phi) + B_1\frac{T_w}{2}\cos(\phi)\dot{\phi} \\ \qquad\qquad +K_1 q_1 - k_1 z_{r1} + k_1 u_1)/m_1 \\ \ddot{z}_{r2} = (B_2\dot{q}_2 - K_2\frac{T_w}{2}\sin(\phi) - B_2\frac{T_w}{2}\cos(\phi)\dot{\phi} \\ \qquad\qquad +K_2 q_2 - k_2 z_{r2} + k_2 u_2)/m_2 \end{cases} \tag{16.6}$$

The normal forces F_{ni}, $i = 1, \cdots, 4$ acting on the wheels are calculated using the following expression:

$$F_{ni} = F_{ci} + k_i(u_i - z_{ri}),\ i = 1, \cdots, 4 \tag{16.7}$$

where F_{ci} is the static force due to the static mass of the vehicle. In this study, the force generated by damping effects is neglected comparing to the spring forces $k_i(u_i - z_{ri})$. On the other hand, the dynamic rolling of the vehicle is described using the following differential equation:

$$I_{xx}\ddot{\phi} = ma_y h\cos(\phi + \varsigma) + mgh\sin(\phi + \varsigma) - C_R\dot{\phi} - K_R\phi \tag{16.8}$$

where I_{xx} is the inertia moment in the roll axis, C_R represents a damping coefficient of the roll motion, K_R is spring coefficient of the roll motion, $\dot{\phi}$ is the roll rate, $\ddot{\phi}$ is the roll acceleration with respect to the road, ς is the lateral slope, h is the centre height of gravity with respect to the roll axis, g represents the gravity acceleration and a_y is the lateral acceleration of the heavy vehicle. This latter variable is calculated during vehicle modelling. It depends on the lateral and longitudinal forces. It can also be measured using accelerometer sensor as described in the following chapter on the experimentation.

16.3 Perturbations and Parameters Identification

Sliding mode based observers are presented as an alternative to the problem of observation of perturbed systems. In particular, High Order Sliding Mode (HOSM) based observers can be considered as a successful technique for the state observation of perturbed systems due to their high precision and robust behavior with respect to parametric uncertainties. In this section, we show how the higher order sliding mode concept can be applied for observation of uncertainties and parameter identification of heavy vehicle ([[29]], [[21]], [[27]]). In order to develop the observer, let us rewrite the equation 16.1 in state form as follows:

$$\begin{cases} \dot{x}_1 = x_2 \\ \dot{x}_2 = f(x_1, x_2) + F_g(x_1, u) \\ y = x_1 \end{cases} \tag{16.9}$$

where $x_1 = [q_1\ q_2\ \phi]$ is the state vector representing the measured outputs vector of the system, x_2 represents its speeds, f is a vector of nonlinear analytical function and F_g is an unknown input vector computed as follows: $F_g = [-F_{g1} - F_{g2}\ 0]^T = [-\frac{F_{Z1}}{m_1}\ -\frac{F_{Z2}}{m_2}\ 0]^T$, where F_{Z1} and F_{Z2} are respectively the right and left impact forces, m_1 and m_2 represent respectively the right and left wheels mass. Before developing the sliding mode observer, let us consider the following assumptions: 1. The state is bounded. 2. The system inputs are bounded. In order to estimate the vertical forces and identify parameters of the system, let us rewrite the system 16.9 :

$$\begin{cases} \dot{x}_{11} = x_{21} \\ \dot{x}_{21} = a_1 \varphi_1(x_{11}) - F_{g1} \\ \dot{x}_{12} = x_{22} \\ \dot{x}_{22} = a_2 \varphi_2(x_{12}) - F_{g2} \end{cases} \tag{16.10}$$

where $x_{11} = q_1, x_{21} = \dot{q}_1, x_{12} = q_2, x_{22} = \dot{q}_2$. The unknown vectors of parameters are represented by a_1 and a_2 such as: $a_1 = \left[k_1(\frac{m_1 - m}{m_1})\ k_2\right]$, $a_2 = \left[k_1\ \ k_2(\frac{m - m_2}{m_2})\right]$, $\varphi_1 = \frac{q_1}{m}$ and $\varphi_2 = \frac{q_2}{m}$. where m represents the unsprung mass of the vehicle. Assuming $(x_1, x_2) = (x_{11}, x_{21})$ or $(x_1, x_2) = (x_{12}, x_{22})$, $\varphi = \varphi_1$ or $\varphi = \varphi_2$ and $a = a_1$ or $a = a_2$,and in order to observe states, the following second order observer is developed: ([[12]], [[10]]) :

$$\begin{cases} \dot{\hat{x}}_1 = \hat{x}_2 + \lambda\, |\tilde{x}_1|^{1/2}\ sign(\tilde{x}_1) \\ \dot{\hat{x}}_2 = \bar{a}\varphi(\hat{x}_1, \hat{x}_2) + \alpha\ sign(\tilde{x}_1) \end{cases} \tag{16.11}$$

where $\hat{x}_1$ and $\hat{x}_2$ are respectively the estimations of x_1 and x_2, $\tilde{x}_1 = x_1 - \hat{x}_1 \in \Re$ is the estimation error, the variable $\bar{a}$ represents a vector of the nominal values of the vector parameters. In this case, the dynamic estimation errors are calculated as follows:

$$\begin{cases} \dot{\tilde{x}}_1 = \tilde{x}_2 - \lambda\, |\tilde{x}_1|^{1/2}\ sign(\tilde{x}_1) \\ \dot{\tilde{x}}_2 = \tilde{a}\ \varphi(x_1, \tilde{x}_2) + \zeta - \alpha\ sign(\tilde{x}_1) \end{cases} \tag{16.12}$$

with $\tilde{a} = a - \bar{a}$ is the estimation error of the vector a, $\zeta = -F_{g1}(x_1,u)$ or $\zeta = -F_{g2}(x_1,u)$ and $\tilde{x}_2 = x_2 - \hat{x}_2$. Since the accelerations of the system are bounded, the variable α can be minored, satisfying the inequality:

$$\alpha > 2\left|\dot{\hat{x}}_2\right| \tag{16.13}$$

On the other hand, from [[11]], the gains of the matrix λ satisfying the inequality, can be selected as :

$$\lambda > \sqrt[2]{\frac{2}{\alpha - 2\left|\dot{\hat{x}}_2\right|}\frac{(\alpha + 2\left|\dot{\hat{x}}_2\right|)(1+p)}{1-p}} \tag{16.14}$$

where $p \in (0,1)$ are some constants to be chosen (proof in ([[10]]). In order to study the observer stability, first, the convergence of $\tilde{x}_1$ and $\dot{\tilde{x}}_1$ to 0 , in finite time t_0 is proved. Then, some conditions about $\tilde{x}_2$ to ensure its convergence to 0 are deduced. Therefore, for $t \geq t_0$ the surface $\tilde{x}_2 = 0$ is attractive, leading $\hat{x}_2$ to converge towards x_2 satisfying the inequalities (16.13) and (16.14). The Super Twisting controller is insensitive to general perturbations $\rho(x_1,S) = F_g(x_1,u)$ satisfying the following conditions:

$$\left\{\begin{array}{l} \rho_1(x_1,S) \leq k_1 |S|^{1/2} \\ \left|\frac{\partial}{\partial t}\rho_2(x_1)\right| \leq k_2 \end{array}\right| \ , \ S = \tilde{x}_1 \tag{16.15}$$

where $\rho(x_1,S) = \rho_1(x_1,S) + \rho_2(x_1)$, $k_1 > 0, k_2 > 0$ As described in [[38]], this is a strong requirement in order to ensure the complete rejection of the disturbance $\rho_1(x_1,S)$ by the Super Twisting algorithm. This allows to develop a general stability proof of this algorithm subject to the general class of disturbances in equation 16.12. The proof is based on the following quadratic Lyapunov function:

$$\left\{\begin{array}{l} V(\zeta,u_1) = \zeta^T P \zeta \\ \zeta = [|S|^{1/2} sign(S), u_1] \\ \dot{u}_1 = -\alpha sign(S) \end{array}\right| \tag{16.16}$$

where $P = P^T > 0$ is a symmetric and positive definite solution of the following linear matrix inequality (LMI), with some constant $\varepsilon > 0$:

$$\begin{bmatrix} A^T P + PA + \varepsilon P + R & PB \\ B^T & -\Theta \end{bmatrix} \leq 0 \tag{16.17}$$

where A is the Hurwitz matrix of the system 16.12:

$$A = \begin{bmatrix} -\lambda & 1 \\ -\alpha & 0 \end{bmatrix} \tag{16.18}$$

In our case, the elements of the gains are $\lambda = 500$ and $\alpha = 1$. The matrices R and Θ take into account the perturbation bounds of the stated problem and can be considered as parameters for observer design and $B = \begin{bmatrix} 1 & 0 \end{bmatrix}^T > 0$. Then, the function 16.16 is a global strong Lyapunov function for the system 16.12. In ([[38]], [[8]]), it is given the proof that the system trajectories under Super Twisting control starting at $S_0 = \begin{bmatrix} S(0) & \dot{S}(0) \end{bmatrix}$ to the origin in finite time when the perturbation $\rho(x_1, S)$ of equation 16.12 is bounded by 16.15. In this case, and from 16.12, one obtains:

$$z_2 = \alpha \; sign(\tilde{x}_1) = \tilde{a} \; \varphi(x_1, \tilde{x}_2) + \zeta \tag{16.19}$$

Theoretically, the equivalent output injection is the result of an infinite switching frequency of the discontinuous term . Nevertheless, the realization of the observer produces a high switching frequency which makes the application of a filter necessary. To eliminate the high frequency component, a filter of the following form is used:

$$\tau \, \dot{\bar{z}}_2(t) = \bar{z}_2(t) + z_2(t) \tag{16.20}$$

where $\tau \in \Re$ and , $h << \tau << 1$ being a sampling step. The variable z_2 is then rewritten as follows:

$$z_2(t) = \bar{z}_2(t) + \xi(t) \tag{16.21}$$

with $\bar{z}_2(t)$ is the filtered version of $z_2(t)$ and $\xi(t)$ is the difference caused by the filtration. Nevertheless, as it is shown in ([[[15]]], [[[42]]]) that:

$$\lim_{\substack{\tau \to 0 \\ h/\tau \to 0}} \bar{z}_2(\tau, h) = z_2(t) \tag{16.22}$$

Thus, it is possible to assume that the equivalent output injection is equal to the output of the filter.

16.3.1 Perturbations Identification

In order identify the perturbation, the vector of parameters a is supposed to be known. In this case $\tilde{a} = 0$. Therefore and using the equation 16.19, the vertical force is obtained as follows:

$$\zeta = \alpha \; sign(\tilde{x}_1) \tag{16.23}$$

One recalls that this perturbation is composed of the impact force or which can be calculated as shown in the equation (16.7). One can then mention the advantages of the proposed method as following: - The measuring of the road profiles u_1 and u_2 is not necessary. - The estimation of the vertical displacements of the wheels and its derivative are also not necessary to obtain.

16.3.2 Parameters Identification

To identify the parameters of the system, we suppose that the perturbation $\zeta = 0$. That means that the road profile is supposed to be close to zero (no irregularities on the road that can affect vertically the vehicle). In this case and using the equation 16.19, we obtain:

$$z_2 = \alpha \; sign(\tilde{x}_1) = \tilde{a} \; \varphi(x_1, \tilde{x}_2) \tag{16.24}$$

Considering the unknown parameters vector a as a constant vector and in order to identify it, a linear regression algorithm, namely the least square method is applied. The time integration is given by:

$$\frac{1}{t}\int_0^t z_2(\sigma)\varphi(\sigma)^T d\sigma = \tilde{a}\frac{1}{t}\int_0^t \varphi(\sigma)\varphi(\sigma)^T d\sigma \tag{16.25}$$

The vector is then estimated by:

$$\overset{\wedge}{\tilde{a}} = \left[\int_0^t z_2(\sigma)\varphi(\sigma)^T d\sigma\right]\left[\int_0^t \varphi(\sigma)\varphi(\sigma)^T d\sigma\right]^{-1} \tag{16.26}$$

where $\overset{\wedge}{\tilde{a}}$ is the estimation of $\tilde{a}$. Let us define

$$\Gamma = \left[\int_0^t \varphi(\sigma)\varphi(\sigma)^T d\sigma\right]^{-1} \tag{16.27}$$

Its derivative is equal to

$$\dot{\Gamma} = -\Gamma\varphi(\sigma)\varphi(\sigma)^T\Gamma \tag{16.28}$$

The derivative of the vector $\overset{\wedge}{\tilde{a}}$ using the equation 16.26 gives:

$$\dot{\overset{\wedge}{\tilde{a}}} = \left[\int_0^t z_2(\sigma)\varphi(\sigma)^T d\sigma\right]\dot{\Gamma} + z_2\varphi(\sigma)^T\Gamma \tag{16.29}$$

Replacing $\dot{\Gamma}$ by its value given before and using the equation 16.26, we obtain:

$$\begin{aligned}\dot{\overset{\wedge}{\tilde{a}}} &= -\overset{\wedge}{\tilde{a}}\varphi\varphi^T\Gamma + z_2\varphi(\sigma)^T\Gamma \\ &= (-\overset{\wedge}{\tilde{a}}\varphi + z_2)\varphi^T\Gamma\end{aligned} \tag{16.30}$$

This ensures the asymptotic convergence of $\overset{\wedge}{\tilde{a}}$ to $\tilde{a}$ and consequently this allows to identify the real value of the vector . In our case, in order to obtain the unsprung masses after identification of $k_1 = a_{12}$ and $k_2 = a_{21}$, we refer to the vector a

defined previously. One notices then the identified values of $a_{11} = k_1(m_1 - m)/m_1$ and $a_{22} = k_2(m_2 - m)/m_2$. Finally, the unsprung masses are deduced as follows: $m_1 = mk_1/(k_1 - a_{11})$ and $m_2 = mk_2/(k_2 - a_{22})$.

16.4 Sliding Mode Observer for Risk Prediction

In order to evaluate the rollover risk, high order sliding mode observer is developed to estimate the state variables and the vertical forces of the vehicle ([42], [35], [11], [25], [17], [30], [26], [28]). In state space form, the system equation (16.1) can be rewritten as:

$$\begin{cases} \dot{x}_1 = x_2 \\ \dot{x}_2 = M^{-1}(F_g - B(x_1, x_2)x_2 - K(x_1)) \end{cases} \tag{16.31}$$

where $x = (x_1, x_2)^T = (q, \dot{q})^T$ is the state variables vector and $x_1 = [q_1, q_2, q_3, q_4, \phi]^T$ is the measured outputs vector of the system. The roll angle is calculated using the following formula:

$$\phi = \arcsin(\frac{q_1 - q_2}{T_w}) \tag{16.32}$$

To be able to estimate the state variables and the vertical forces, the following observer is developed and the convergence is proved ([36], [17]).

$$\begin{cases} \dot{\hat{x}}_1 = \hat{x}_2 - \lambda_0 |\hat{x}_1 - x_1|^{2/3} sign(\hat{x}_1 - x_1) \\ \dot{\hat{x}}_2 = \hat{x}_3 - \lambda_1 \left|\hat{x}_2 - \dot{\hat{x}}_1\right|^{1/2} sign(\hat{x}_2 - \dot{\hat{x}}_1) \\ \dot{\hat{x}}_3 = -\lambda_2 sign(\hat{x}_3 - \dot{\hat{x}}_2) \end{cases} . \tag{16.33}$$

where $\hat{x}_1$, $\hat{x}_2$ and $\hat{x}_3$ are respectively the estimate of x_1, x_2 and $\dot{x}_2$, λ_0, λ_1 and λ_2 are the observer gains. More details about this observer can be found in [35]. The observer defined in (16.33) permits to estimate positions, velocities and accelerations of the system. The jerk of the system is bounded and it satisfies the inequality:

$$f^+ \geq 2\left|\dddot{x}_1\right| \tag{16.34}$$

where f^+ is some known positive scalar. The estimation errors are obtained using the equations (16.31) and (16.33) as following:

$$\begin{cases} \dot{\tilde{x}}_1 = x_2 - \hat{x}_2 + \lambda_0 |\hat{x}_1 - x_1|^{2/3} sign(\hat{x}_1 - x_1) \\ \dot{\tilde{x}}_2 = \dot{x}_2 - \hat{x}_3 + \lambda_1 \left|\hat{x}_2 - \dot{\hat{x}}_1\right|^{1/2} sign(\hat{x}_2 - \dot{\hat{x}}_1) \\ \dot{\tilde{x}}_3 = \ddot{x}_2 + \lambda_2 sign(\hat{x}_3 - \dot{\hat{x}}_2) \end{cases} \tag{16.35}$$

where $\tilde{x}_i = x_i - \hat{x}_i$ $(i = 1, \cdots, 3)$ is the estimation error of the variable x_i. Chosen the i^{th} components of λ_0, λ_1 and λ_2 as: $\lambda_0 = 3\sqrt[3]{f^+}$, $\lambda_1 = 1.5\sqrt[2]{f^+}$ and $\lambda_2 = 1.1f^+$, the estimation errors $\tilde{x}_1$, $\tilde{x}_2$ and $\tilde{x}_3$ converge in finite time t_0 toward 0 . More details about the convergence study of this observer can be found in [16]. In this case, by

means of the equation (16.6), the vertical displacements of the wheels are estimated in finite time, since the vertical accelerations of the wheels $\ddot{z}_{ri}$ are measured using accelerometers:

$$\begin{cases} \hat{z}_{r1} = (-m_1\ddot{z}_{r1} + B_1\dot{\hat{q}}_1 + K_1\frac{T_w}{2}\sin(\hat{\phi}) \\ +B_1\frac{T_w}{2}\cos(\hat{\phi})\dot{\hat{\phi}} + K_1\hat{q}_1 + k_1u_1)/k_1 \\ \\ \hat{z}_{r2} = (-m_2\ddot{z}_{r2} + B_2\dot{\hat{q}}_2 - K_2\frac{T_w}{2}\sin(\hat{\phi}) \\ -B_2\frac{T_w}{2}\cos(\hat{\phi})\dot{\hat{\phi}} + K_2\hat{q}_2 + k_2u_2)/k_4 \end{cases} \tag{16.36}$$

From equation (16.5), the centre height of gravity $\hat{z}$ is now deduced :

$$\hat{z} = \frac{1}{2}(\hat{z}_{r1} + \hat{z}_{r2} + \hat{q}_1 + \hat{q}_2) + q_0 + r \tag{16.37}$$

Using the equation (16.7), the vertical forces F_{ni} can be estimated by:

$$\hat{F}_{ni} = F_{ci} + k_i(u_i - \hat{z}_{ri}),\ i = 1, \cdots, 4 \tag{16.38}$$

Then the Load Transfer Ratio (LTR) used to indicate the rollover risk, is calculated as follows [[1]]:

$$LTR = \frac{F_{nr} - F_{nl}}{F_{nr} + F_{nl}} \tag{16.39}$$

When $F_{nr} = 0$ ($F_{nl} = 0$) the right (left) wheels lift off the road and the rollover coefficient takes on the limit value $LTR = -1$ ($LTR = 1$). For straight driving on a horizontal road for the tire vertical forces, it holds that $F_{nr} = F_{nl}$ which means that $LTR = 0$.

16.5 Experimental Results

16.5.1 Description of the Test Bench

In order to validate theoretical study and the simulations results, an instrumented tractor of Renault Trucks company is used, as shown in figure 16.1. The vehicle is equipped with several sensors to measure the dynamics of the vehicle, such as the angular speeds, accelerations, and the suspension deflections. The figure 16.3 illustrates the added sensors which are needed for the proposed technique:

- Four sensors, LVDT (Linear Variable Differential Transformers) installed between the wheel and the chassis in order to measure the deflections of suspensions,

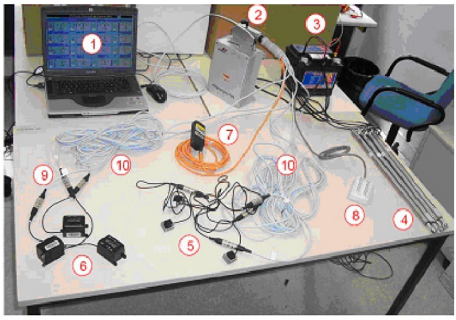

1. Control desk software
2. Micro-Autobox
3. Battery
4. LVDT sensors
5. Accelerometers
6. Gyrometers
7. Laser sensor
8. BNC connectors

Fig. 16.3 The used sensors on the Vehicle

- Four accelerometers installed on the chassis in order to measure the vertical accelerations of wheels,
- Three axial gyrometers installed on the chassis in order to measure the angular speeds (roll, pitch and yaw rate),
- Two lasers installed at the bottom of the chassis in order to measure its height.

The figure 16.4 illustrates the positions of installed sensors in the vehicle. Two LVDT sensors are installed in the front of the vehicle and two others are installed in the rear of the tractor. The two laser sensors are installed respectively in the left and in the right side in order to measure the height of the vehicle. The tri-axial gyrometer is installed in the centre of the vehicle in order to measure the three rotations of the tractor.

The LVDT are the only sensors which are necessary and needed to be added in order to product the predictive rollover system. The roll angle is deduced using LVDT sensors, as explained in the previous section. The other sensors are only used in order to test the robustness of the approach by comparing their measures to the estimated variables.

The acquisition part of the bench, consists of use of laptop computer, a dSPACE Micro AutoBox real-time hardware system, and the software: Matlab/Simulink, Real Time Workshop and the dSPACE acquisition system. This acquisition board delivers high performance and reliable data acquisition capabilities with 16 single-ended analogical inputs. It delivers both analogical and digital triggering capability, as well as two 12-bit analogical outputs, two 24-bit and 8 digital I/O lines. The sampling frequency used during the tests is 100 Hz.The algorithms were written in Matlab/Simulink, which coordinates all the data acquisition and the test measurement processes. The developed program can be easily manipulated and integrated in the vehicle.

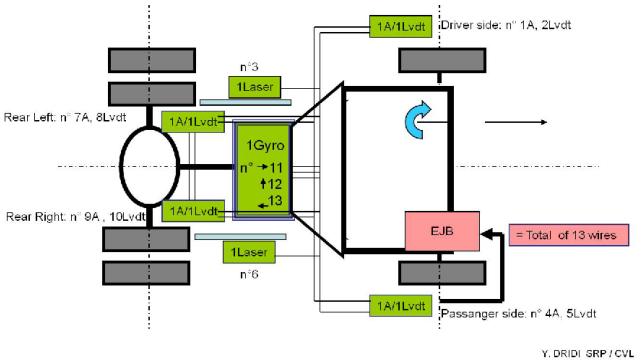

Fig. 16.4 Sensors position on the heavy vehicle

16.5.2 Infrastructure Measurements

Before the tests, the infrastructure data have been measured by different devices. The road profile is measured by Longitudinal Profile Analyzer shown in figure 16.5. The technical description and the functionalities of this device are given in [34]. The radius of curvature, longitudinal and lateral slope are measured using VANI (Véhicule d'Analyse d'Itinéraire).

Fig. 16.5 Longitudinal Profile Analyser

This vehicle is equipped with different sensors, such as Gyrometers, GPS and lasers is realized by Regional Laboratory of Lyon, in France in 1987. The CFT

(transversal friction coefficient) of the road surface is measured by SCRIM device (Sideway force Coefficient Routine Investigation Machine) which is described in *http://www.vectra.fr*.

16.5.3 Test Results

Many tests and scenarios have been realized with the instrumented vehicle driving at various speeds. Some results on the states, the vertical forces and the risk estimations are presented in this section. The dynamic parameters and the static vertical forces are measured before the tests. The measured static front left and static right vertical forces are respectively 24200N and 25250N. The values of static rear left and right vertical forces are respectively 9450N and 12050N.

16.5.3.1 Zigzag Test

The zigzag test is illustrated by figure 16.6. This test is very interesting for rollover study since it can cause dangerous situations. The driver changes abruptly the direction of his vehicle which implies load transfer between the left and right side of the vehicle.

Fig. 16.6 The zigzag test in practise

The steering angle of the vehicle during this test is presented in the figure 16.7. The critical times are occurred at 15s, 30s and 45s. One notices that at these times, the absolute steering angle is more than 3rad (180). In order to verify the condition 16.34, let us represent the jerk of the systems which corresponds to the double

derivative of roll rate measured by gyrometer sensor and the jerk coming from the third derivative of suspension deflection, measured by LVDT sensor. The result is shown in the figure 16.8.

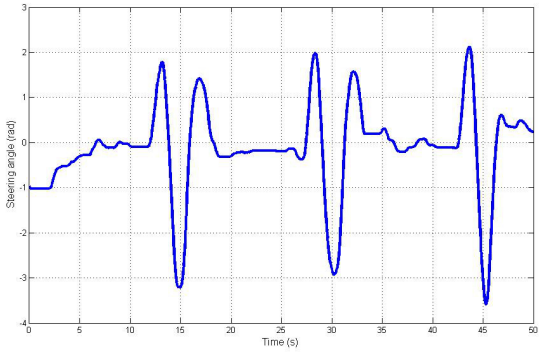

Fig. 16.7 Steering angle for zigzag test

One remarks that the maximum values of jerks of suspension deflection and roll angle are respectively $800m/s^3$ and $150rad/s^3$. In this case, the value of the gain f^+ is then deduced to be equal to 1600. The vehicle speed is shown in figure 16.9.

In the figure 16.10, suspension deflections of the front of the vehicle are estimated and compared to the measured one.

This figure shows that the observer converges quickly and the estimation error is around zero. Therefore, the two graphs are practically indistinguishable. At the critical times, the effect of the zigzag on the vehicle dynamics is clearly shown at $15s$, $30s$ and $45s$. The suspension deflection at the front right decreases from its static value $0.01m$ to $-0.03m$, whereas the suspension deflection at the front left increases from $0.01m$ to $0.025m$. From this behavior, the roll angle shown in the figure 16.11 occurred. Indeed, at the times $15s$, $30s$ and $45s$, the roll angle increased. One can notice the quality of the estimation compared to the measure. It is clearly shown that the estimated and measured roll angles are in good agreement.

The figure 16.12 shows the estimation of the centre height of gravity compared to the front left suspension deflection. Since, there is no existing sensor to measure this displacement, it's then difficult to judge the quality of the estimation.

However, one notices that at $15s$, the suspension deflection increased up to $0.025m$ and at the same time, the estimated centre height of gravity increased up to $0.71m$. The same phenomena are produced at the times $30s$ and $45s$. This implies that the estimated centre height of gravity correctly tracks the LVDT measure. This conclusion represents a good indicator to evaluate the quality of this estimation. In the figure 16.13, the vertical forces of the front wheels are presented. The force of the front left wheel is presented at the left.

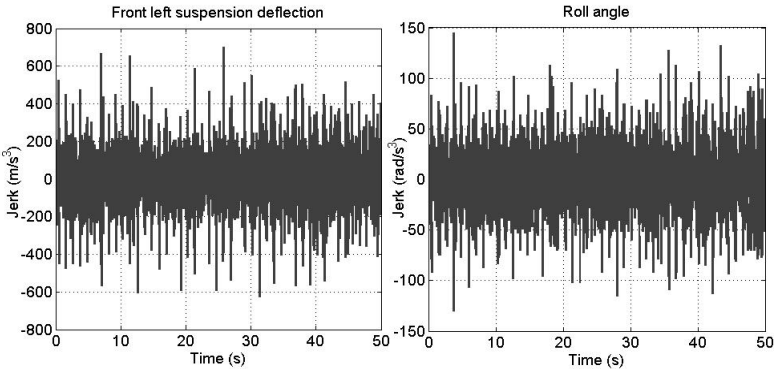

Fig. 16.8 Jerk of the system in case of zigzag test

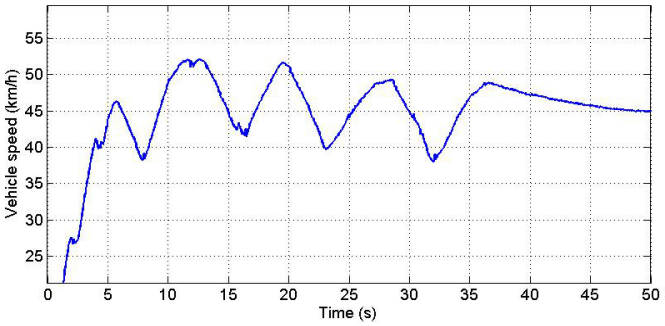

Fig. 16.9 Vehicle speed for zigzag test

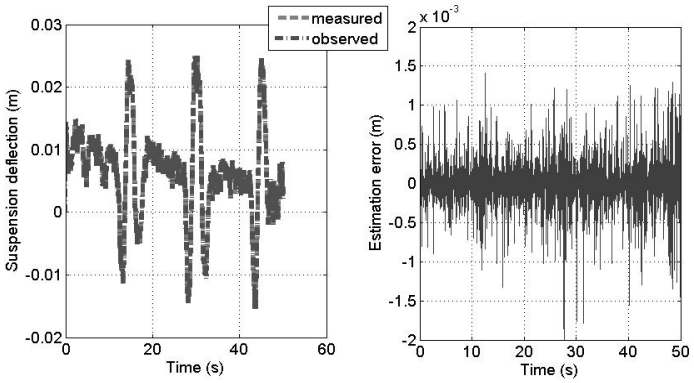

Fig. 16.10 Suspension deflection estimation

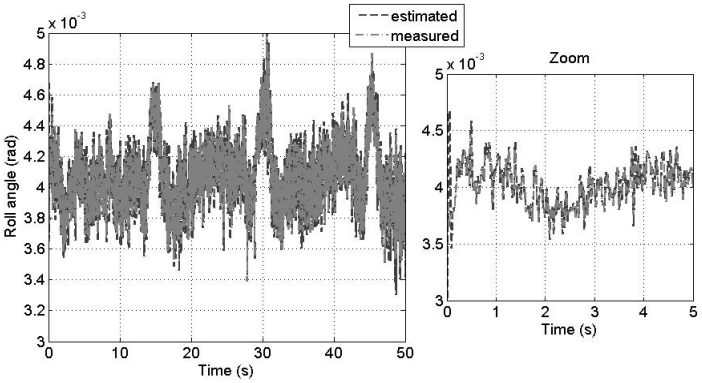

Fig. 16.11 Roll angle estimation

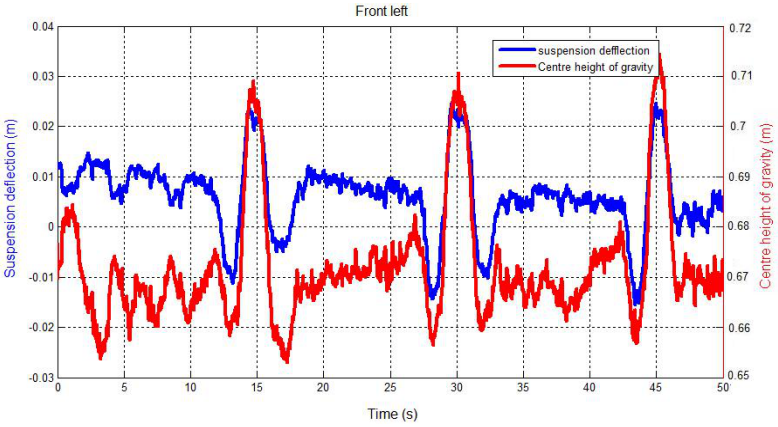

Fig. 16.12 Estimation of centre height of gravity

One notices that at the times $15s$, $30s$ and $45s$, this force increases up to $28dN$ following then the the measured suspension deflection.

A zoom on the time interval $[0\ 5]s$ is given in the right side of this figure 16.13. The figure 16.14 shows the estimated vertical force of the front right wheel.

As explained before, the same conclusion can be given here. indeed, at the same times, this force decreases up to $19dN$. This phenomena can be explained by the fact, that the load transfer from the right side to the left side of the vehicle is produced. A zoom on the time interval $[0\ 5]s$ is given in the right side of th figure 16.14.

In the figure 16.15, the vertical forces are compared to suspension deflections measures. As for the centre height of gravity, there are no sensors, during this test, to measure the vertical forces. It's then difficult to conclude on the quality of the

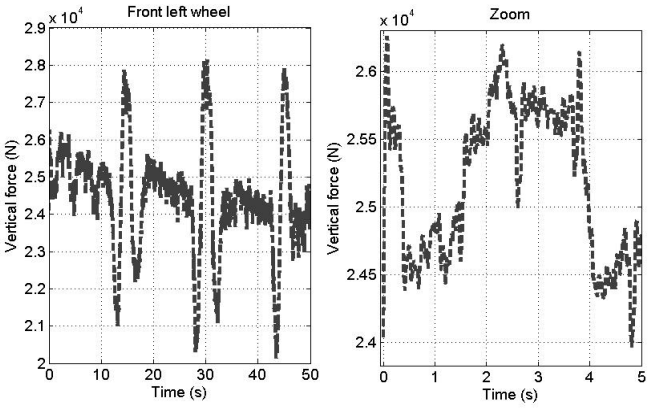

Fig. 16.13 Estimation of vertical force: left wheel

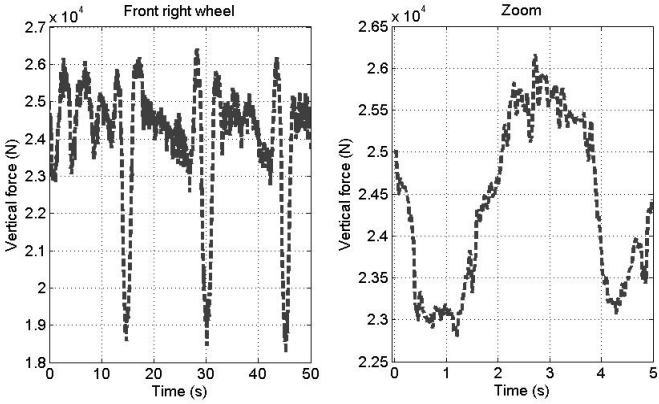

Fig. 16.14 Estimation of vertical force: right wheel

estimation. However, it is clearly shown that the estimated forces and the equivalent measured suspension deflections are well correlated. This gives us an idea about the quality of estimation. From figures 16.15, the load transfer ratio between the two wheels is calculated and shown in the figure 16.16. The values of LTR are situated between -0.15 and 0.2 .

These values are much smaller than the risk limit LTR=1, where on wheel of the same axle lifts off the road. This is due to the fact that, during the test and for safety reasons, the driver is not allowed to reach this limit. However, in order to test the approach and send an alarm to the driver, the coefficient limit of LTR is reduced to 0.2. In the figure 16.17, the identification results are shown. The suspensions stiffness k_1 and k_2 are identified with success. Compared to their nominal values

(194680N/m and 188540N/m), these parameters have been identified with some variation in the time interval $[13,20]s$. This is due to the fact that at this time, the driver changes brutally the vehicle direction as shown in the steering angle of the Figure 16.7.

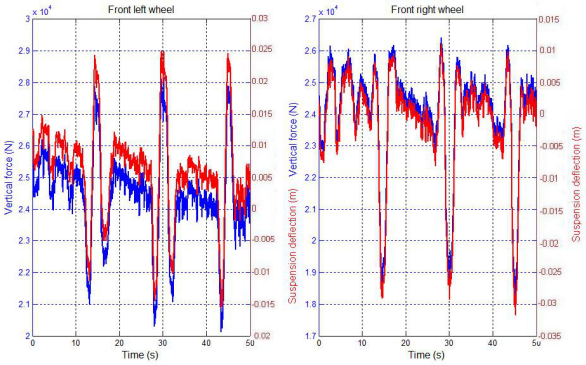

Fig. 16.15 Vertical forces estimation compared to LVDT measures

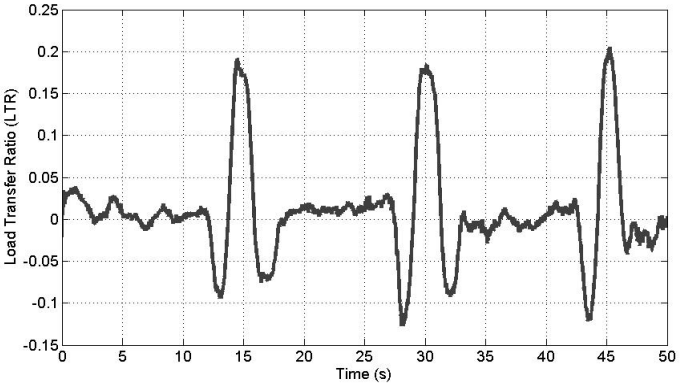

Fig. 16.16 Load Transfer Ratio (LTR)

The same remark can be given to the unsprung masses identification m_1 and m_2. The variation of these parameters occurs around their nominal values respectively of $100kg$ and $95kg$, at the same time interval $[13,20]s$.

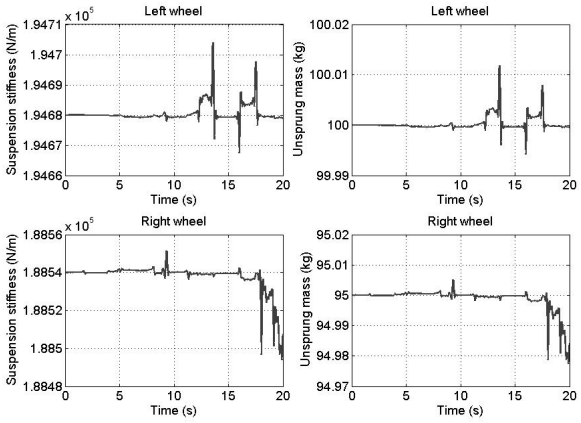

Fig. 16.17 Parameters identification

16.5.3.2 Braking test

In this section, the brake test is presented in order to show the rapidity and the robustness of the proposed method using observers. This test allow us to know if the rollover risk can occur in the case of braking. In the figure 16.18, the vehicle speed during this test is shown. The braking occurs at times $9s$, $29s$ and $49s$.

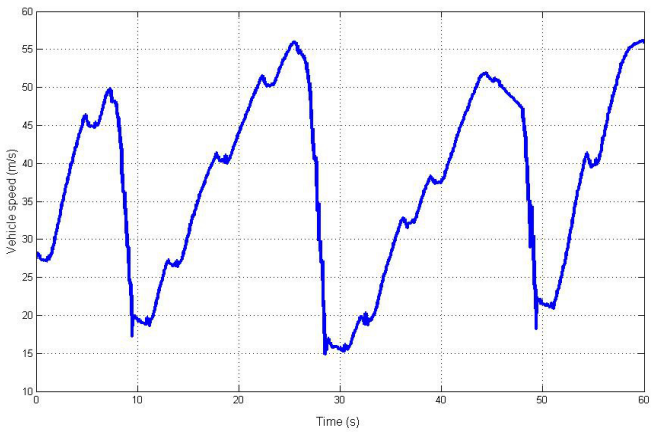

Fig. 16.18 Vehicle speed for brake test

In the following, the influence of the braking on the vehicle behavior and the rollover risk is shown.

In this case, the jerk of the system which corresponds to the double derivative of roll rate measured by gyrometer sensor and the jerk coming from the third derivative of suspension deflection measured by LVDT sensor are shown in the figure 16.19. One remarks that the jerks of suspension deflection and roll angle are respectively bounded by $800m/s^3$ and $250rad/s^3$. Also in this case, the value of the gain f^+ is chosen to be equal to 1600.

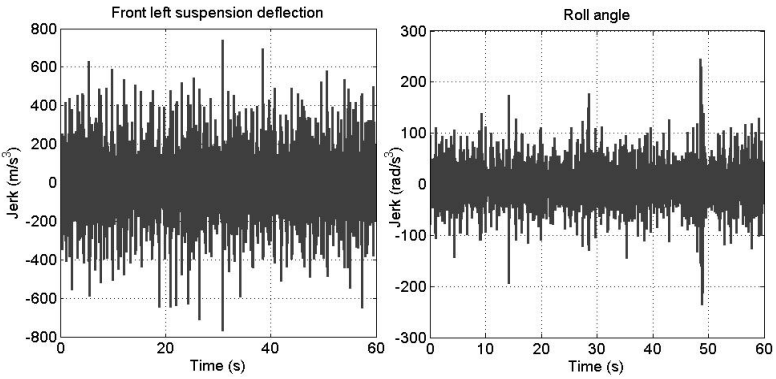

Fig. 16.19 Jerk in the brake test

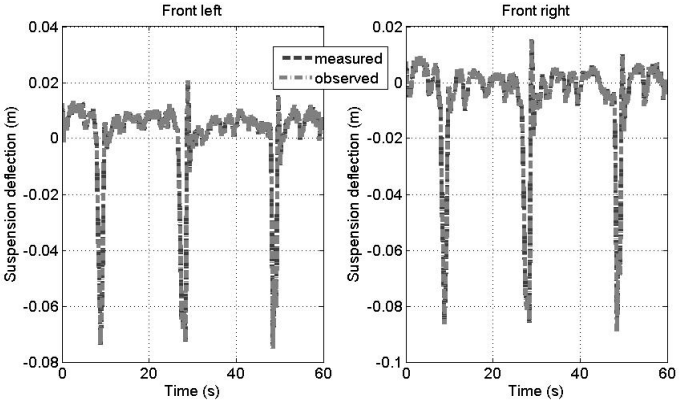

Fig. 16.20 Suspension deflection estimation

In the figure 16.20, the estimation of the suspension deflections of the front of vehicle are represented and compared to measures. At the braking times $9s$, $29s$ and $49s$, these vertical displacements decrease.

The right and the left side have almost the same value of about $-0.08m$. In this case no load transfer is occurred between the left and the right side of the vehicle.

To show the quality estimation of the roll angle, a zoom is done in the time interval $[0\ 2]s$ of the figure 16.21. One notices that in this case, the roll angle is not

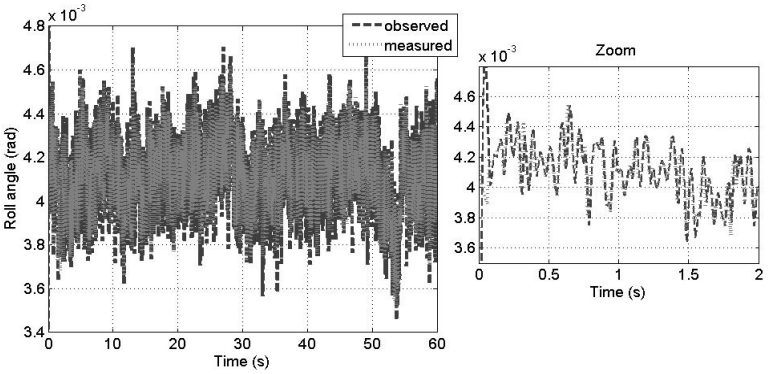

Fig. 16.21 Roll angle estimation

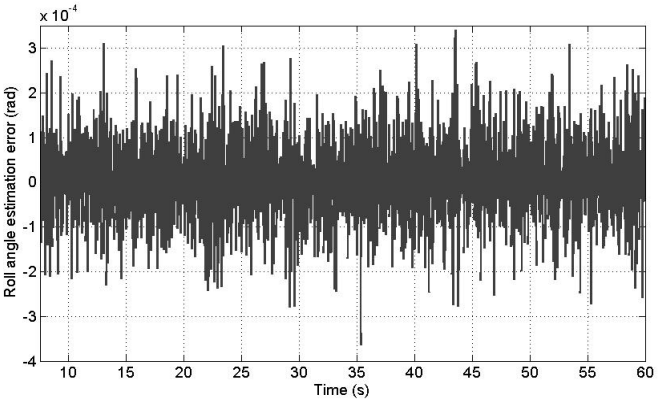

Fig. 16.22 Roll angle estimation error

high even in the braking times. The estimation error tends to zero as shown in the figure 16.22. The maximum value is around $10^{-4} rad$.

The figure 16.23 shows that the estimated roll rate compared to the gyrometer's measure. One remarks that the estimation converges quickly toward the measure.

Indeed, the minimum value for the measured roll rate is about $-0.03 rad/s$ and for the estimated roll rate is about $-0.04 rad/s$. The maximum value is almost the same for the two signals. It's about $0.03 rad/s$. The estimation error is shown in the figure 16.24.

The figure 16.25 shows the estimation of the centre height of gravity. At the braking times $9s$, $29s$ and $49s$, the centre height of gravity increased up to $0.8m$ and between these times, the value of this displacement stays at its static value, namely $0.68m$.

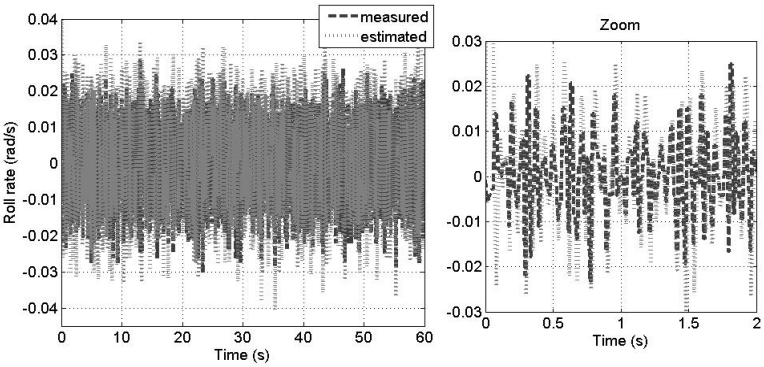

Fig. 16.23 Roll rate estimation in the case of brake test

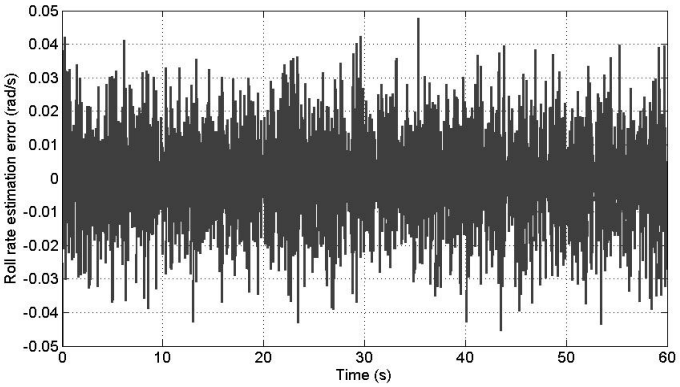

Fig. 16.24 Roll rate estimation error

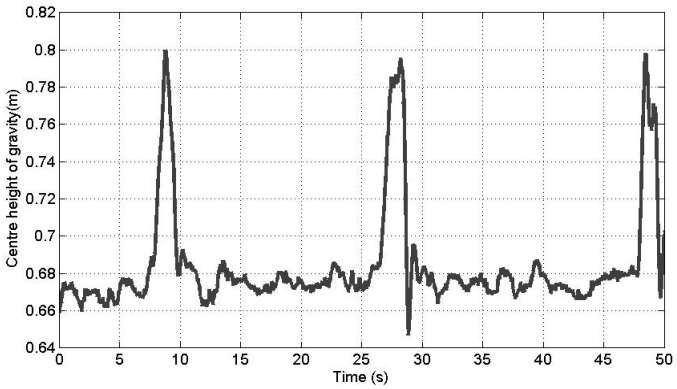

Fig. 16.25 Estimation of centre height of gravity

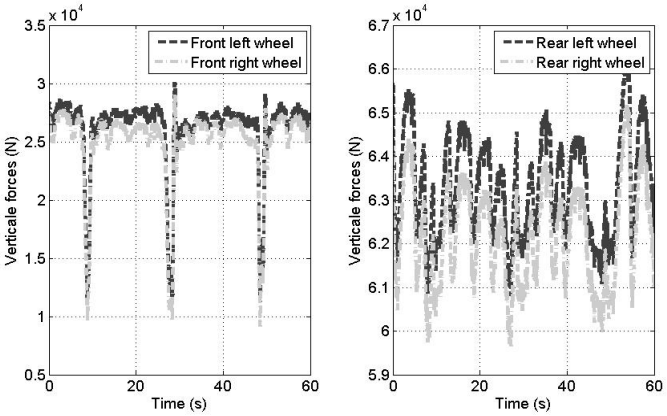

Fig. 16.26 Estimation of vertical forces in case of brake test

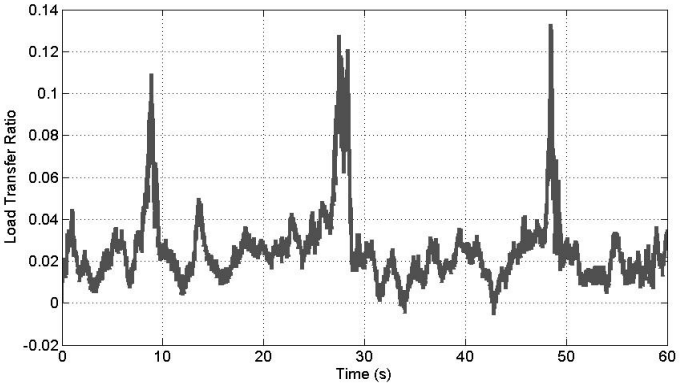

Fig. 16.27 Load Transfer Ratio for brake test

In the figure 16.26, the vertical forces of the wheels are presented. In the left, the front left and right forces are presented. One notices that these forces are quit close. That is confirmed by the small value of the roll angle shown previously in the Figure 16.21.

The second remark, is about the values of these two forces at the times 9*sec*, 29*sec* and 49*sec*, which decrease to 8000*N*. Between these times, the forces keep their static values.

In the right of the figure 16.26, the rear left and right forces are shown. These forces vary around their static values, which is conform to the braking test. The figure 16.27 shows the Load Transfer Ratio (LTR).

One notices an increase of its value from 0.02 until respectively 0.11, 0.13 and 0.135, at braking times, respectively $9sec$, $29sec$ and $49sec$. However, these values still far from the limit value of 1 and the limit fixed in this work, namely 0.2. In this condition, no rollover risk is detected and therefore, no alarm is sent to the driver.

16.6 Conclusion

In this work, an original system of heavy vehicles rollover risk prediction has been proposed. The main advantage of the method is its simplicity and it is based on vertical forces estimation using high order sliding mode observer. It has been validated experimentally on a real heavy truck rolling on the road at various speeds and lane-change manoeuvres. Good agreement has been shown between the experimental and theoretical results. In order to show the robustness of the proposed approach, two tests are presented in this study: zigzag and brake test. The results show that dynamic states are well estimated as shown in the centre height of gravity. Then, vertical forces are estimated and the rollover indicator LTR is computed. The results have been discussed. It is shown that the estimation results are quite close to experimental ones and the rollover is predicted. In this test, the LTR does not reach its limit of 1. In the real situation and for safety reason and only for this reason, we were not allowed to test this situation where one wheel lifts of the road because the tractor is not equipped with safety device. However, in order to send an alarm to the driver and to test its effect on the driver's behavior, this limit is reduced to 0.2. For this reason, the LTR limit to send the alarm is reduced to 0.2. In this case, and during the zigzag test, this limit is reached and the alarm is then sent to the driver in order to reduce his speed. The method proved in the case of brake test, that no rollover occurs ($LTR < 0.2$). HOSMO are also employed in order to estimate vertical forces of heavy vehicle and to identify the unknown parameters. The experimental tests carried out on an instrumented tractor show the quality of this approach since the convergence of the observer is quick and is done in finite time, with errors quite close to zero. The vertical forces are also well estimated. This is noticed when the estimations are compared to the measures. The originality of this approach is the use of the equivalent control, which provides a linear regression algorithm in order to identify the unknown parameters of the system. An example of identification of the unsprung mass and the stiffness is given in this paper. In the future work, it will be interesting to test this approach in real time with an instrumented vehicle. The dynamo wheel in order to measure the impact forces will be useful in order to have a better reference to validate the impact forces estimation. The proposed method is tested on an instrumented tractor. It can be interesting to test the robustness of this approach on tractor semi-trailer.

References

1. Ackermann, J., Odenthal, D.: Damping of vehicle roll dynamics by speed-scheduled active steering. In: European Control Conference, Karlsruhe, Germany (1999)
2. Ahrens, J.H., Khalil, H.K.: High-gain observers in the presence of measurement noise: A switched-gain approach. Automatica 45(4), 936–943 (2009)
3. Cebon, D.: Interaction between heavy vehicles and roads. In: Society of Automotive Engineers, USA, pp. SP–931, 81 (1993)
4. Chen, B.C., Peng, H.: A real-time rollover threat index for sports utiliy vehicles. In: American Control Conference, San Diego, USA, pp. 1233–1237 (1999)
5. Chen, B.C., Peng, H.: Rollover warning of articulated vehicles based on a time-to-rollover metric. In: Proc. ASME Int. Congress and Exploitation (1999)
6. Chen, C., Tomizuka, M.: Dynamic modeling of articulated vehicles for automated highway systems. In: American Control Conference, pp. 653–657 (1995)
7. Dakhlallah, J., Imine, H., Sellami, Y., Bellot, D.: Heavy vehicle state estimation and rollover risk evaluation using kalman filter and sliding mode observer. In: IEEE European Control Conference, ECC 2007, Kos, Grece, pp. 3444–3449 (2007)
8. Davila, A., Moreno, J., Fridman, L.: Variable gains super-twisting algorithm: A lyapunov based design. In: IEEE American Control Conference (2011)
9. Davila, J., Fridman, L., Levant, A.: High-order sliding observation and fault detection. In: 16th Mediterranean Conference on Control and Automation, Ajaccio, Corsica, France, pp. 1699–1704 (2008)
10. Davila, J., Fridman, L., Poznyak, A.: Observation and identification of mechanical systems via second order sliding modes. In: 2006 International Workshop on Variable Structure Systems, VSS 2006, Sardinia, Italy, pp. 232–237 (2006)
11. Davila, J., Fridman, L., Poznyak, A.: Observation and identification of mechanical systems via second order sliding modes. International Journal of Control 79(10), 1251–1262 (2006)
12. Emelyanov, S.V., Korovin, S.K., Levantovsky, L.V.: Second order sliding modes in controlling uncertain systems. Soviet Journal of Computer and System Science, 63–68 (1986)
13. Evans, J., Batzer, S., Andrews, S.: Evaluation of heavy truck rollover accidents. In: 19th International Safety Conference on the Enhanced Safety of Vehicles, Washington DC, USA, pp. 05–0140–W (2005)
14. Floret-Pontet, F., Lamnabhi-Lagarrigue, F.: Parameter identification methodology using sliding mode observers. Int. Journal of Control 74(18), 1743–1753 (2001)
15. Fridman, L.: The Problem of Chattering: An Averaging Approach. In: Young, K., Ozguner, U. (eds.) Variable Structure, Sliding Mode and Nonlinear Control. LNCIS, vol. 247, pp. 363–386. Springer, Heidelberg (1999)
16. Fridman, L., Levant, A., Davila, J.: High-order sliding-mode observation and identification for linear systems with unknown inputs. In: Proc. 45th IEEE Conf. Decision Control, San Diego, CA, USA, pp. 5567–5572 (2006)
17. Fridman, L., Shtessel, Y., Edwards, C., Yan, X.: Higher-order sliding-mode observer for state estimation and input reconstruction in nonlinear systems. Int. J. Robust Nonlinear Control 18(4-5), 399–413 (2008)
18. Gaspar, P., Szaszi, I., Bokor, J.: Reconfigurable control structure to prevent the rollover of heavy vehicles. Control Engineering Practice (13), 699–711 (2005)
19. Gillespie, T.D., Karamihas, S.M.: Characterising trucks for dynamic load prediction. Int. J. Vehicle Design 1(1), 3–19 (1993)

20. Ibrahim, I.M.: Design of reducing the generated dynamic tyre loads of the articulated tanker vehicles. Int. J. of Vehicle Design Heavy Vehicle Systems 11(1), 86–99 (2004)
21. Imine, H.: Identification of heavy vehicle parameters and steering control for rollover avoidance. In: IAVSD, International Symposium on Dynamics of Vehicles on Roads and Tracks, Manchester, UK (2011)
22. Imine, H., Dolcemascolo, V.: Influence of the road profile on wheel and vehicle loads estimation. In: 9th International Symposium on Heavy Vehicle Weights and Dimensions, Pennsylvania, USA (2006)
23. Imine, H., Dolcemascolo, V.: Vertical tyre forces estimation to calculate the rollover risk of heavy vehicles. In: FISITA 2006, World Automotive Congress, Yokohama, Japan, Yokohama, Japan, p. F2006V078 (2006)
24. Imine, H., Dolcemascolo, V.: Warning system to prevent rollover of heavy vehicles. In: 9th International Symposium on Heavy Vehicle Weights and Dimensions. Pennsylvania, USA (2006)
25. Imine, H., Dolcemascolo, V.: Rollover risk prediction of heavy vehicle in interaction with infrastructure. IJHVS, International Journal of Heavy Vehicle Systems 14(3), 294–307 (2007)
26. Imine, H., Dolcemascolo, V.: Sliding mode observers to heavy vehicle vertical forces estimation. IJHVS, International Journal of Heavy Vehicle Systems 15(1), 53–64 (2008)
27. Imine, H., Fridman, L., Shraim, H.: Identification of heavy vehicle suspension parameters and estimation of vertical forces. In: VSS 2012, International Workshop on Variable Structure Systems, Bombay, India, pp. 63–69 (2012)
28. Imine, H., Fridman, L., Sraim, H., Djemai, M.: Sliding Mode Based Analysis and Identification of Vehicle Dynamics. LNCIS, vol. 414. Springer, Heidelberg (2011)
29. Imine, H., Khemoudj, O.: Dynamic parameters identification and estimation of the vertical forces of heavy vehicle. In: SAE 2011 World Congress on Automotive, Detroit, USA (2011)
30. Imine, H., Madani, T., Srairi, S.: High order sliding mode observers to estimate vertical forces: experimental results. In: ITSC, IEEE Intelligent Transportation Systems Society, Beijing, China, pp. 523–527 (2008)
31. Johansson, B., Gafvert, M.: Untripped suv rollover detection and prevention. In: 43rd IEEE Conference on Decision and Control, Atlantis, Paradise Island, Bahamas, pp. 5461–5466 (2004)
32. Khemoudj, O., Imine, H., Djema, M.: Robust observation of tractor-trailer vertical forces using inverse model and exact differentiator. SAE, International Journal of Materials and Manufacturing 3(1), 278–289 (2010)
33. Khemoudj, O., Imine, H., Djemai, M., Fridman, L.: Variable gain sliding mode observer for heavy duty vehicle tyre forces estimation. In: 11th International Workshop on Variable Structure Systems, VSS 2010, pp. 522–527. Mexico city, Mexico (2010)
34. Legeay, V., Daburon, P., Gourraud, C.: Comparaison de mesures de l'uni par l'analyseur de profil en long et par compensation dynamique. Bulletin interne, Laboratoire Central des Ponts et Chaussées, DGER/IRVAR (1996)
35. Levant, A.: Sliding order and sliding accuracy in sliding mode control. International Journal of Control 58, 1247–1263 (1993)
36. Levant, A.: Robust exact differentiation via sliding mode technique. Automatica 34(3), 379–384 (1998)
37. Levant, A.: High-order sliding modes: differentiation and output-feedback control. International Journal of Control 76(9-10), 924–941 (2003)
38. Moreno, J.: Lyapunov Approach for Analysis and Design of Second Order Sliding Mode Algorithms, ch. 4, pp. 122–150. Springer (2011)

39. ONISR: La sécurité routiére en france. bilan de l'année 2004. La documentation franccaise, sécurité routiére, Observatoire National Interministériel de sécurité routiére (2005)
40. Soderstrom, T., Stoica, P.: System Identification. Prentice Hall International, Cambridge (1989)
41. Tianjun, Z., Zong, C., Zheng, H., Tian, C., Zheng, H.: Yaw/roll stability modeling analyses and control of heavy tractor-semitrailer. In: SAE Intl. Asia Pacific Automotive Eng. Conf. (2007)
42. Utkin, V.: Sliding Modes in Control and Optimization. Springer, Berlin (1992)
43. Vasiljevic, L.K., Khalil, H.K.: Error bounds in differentiation of noisy signals by high-gain observers. Systems and Control Letters 57, 856–862 (2008)